

# Experiment research on overburden mining-induced fracture evolution and its fractal characteristics in ascending mining

Cheng Wang · Nianchao Zhang · Yafeng Han ·  
Zuqiang Xiong · Deyu Qian

Received: 21 June 2013 / Accepted: 4 November 2013 / Published online: 21 November 2013  
© Saudi Society for Geosciences 2013

**Abstract** The simulated material model was used to simulate the formation and distribution of overburden fractures induced by ascending mining. The fracture evolution law was revealed. The fractal geometry theory and MATLAB software were applied to analyze fractal characteristics of fracture network of overburden stratum. The results showed that the overburden failure evolution is trapezoidal, accompanied with collapse in layer group and the developing height of fractures discontinuously jumps; as the mining width increased, the fractal dimension of fracture network showed an overall ascending trend, presenting three stages, namely, fast dimension rising stage, slow dimension rising stage, and stable stage. In the caving zone, fracture zone, and bending zone, the development, propagation, and closure of fractures were asynchronous and inner similar. These achievements are important to roof roadway stability control and layout of gas drainage system and contribute to the simultaneous extraction theory of coal and gas by pressure relief.

**Keywords** Ascending mining · Overburden strata · Mining-induced fracture evolution · Fractal dimension

C. Wang · Y. Han · Z. Xiong  
School of Energy Science and Engineering, Henan Polytechnic University, Jiaozuo, Henan 454000, China

N. Zhang (✉)  
School of Mines, Key Laboratory of Deep Coal Resource Mining, Ministry of Education, China University of Mining and Technology, Xuzhou, Jiangsu 221116, China  
e-mail: znc357711543@hotmail.com

N. Zhang  
School of Earth Sciences, University of Queensland, St Lucia, Queensland 4072, Australia

D. Qian  
Department of Earth Resources Engineering, Faculty of Engineering, Kyushu University, Fukuoka 819-0395, Japan

## Introduction

With the increasing demand of coal, the shallow resources were gradually reduced and depleted, with the depth of coal mines becoming increasingly deeper, such as Xuzhou, Kailuan, Huainan, and Xinwen mining areas, and have entered the deep mining, with the mining depths more than 800 m, even up to 1,200 m (Li et al. 2005; Liu et al. 2004). Most deep coal mines in China are multilayer coal seam longwall mining, generally with complex structures, soft coal, high gas, and low permeability characteristics (Ye et al. 1999). Therefore, the mining difficulty of deep mining especially in high-gas coal mine increases, intensifying the mining risk and cost.

Because of the low permeability and high-gas content of deep multilayer coal seam longwall mining, the long-term theoretical research and highly dangerous coal seam mining practice prove that the pressure relief antireflection effect caused by ascending mining can be employed for coal and gas simultaneous extraction which is the best way of coal mine gas disaster prevention and environmental protection in China. Upward mining has been widely used and gradually become a routine mining technology (Hu et al. 2009; Cheng and Yu 2007; Liu et al. 2009; Ma et al. 2008; Yuan 2009; Wang et al. 2011). In ascending mining, after the target coal seam has been extracted, the gravity of the roof rock causes the periodic caving and fracturing of the immediate and main roof and the deformation, failure, and movement of the overlying rock beds, forming a crack network (Qian and Shi 2003). The law of crack distribution and evolution which determines the layout of gas pressure relief and gas drainage boreholes becomes the main controlling factor of the roof stability influence (Wang 2011). Therefore, it is necessary to carry out studies on the overburden fracture distribution and evolution in ascending mining.

In modern mining engineering programs, physical simulation, numerical simulation, and field observation are the most common research methods. Field observation is necessary, but it has a lot of disadvantages, such as costing a lot of money and time, dirty underground site, dangerous, etc. (Liu et al. 2003), especially because you cannot watch through the surrounding rocks to see what is happening in the roof beds. Numerical simulation is a burgeoning and simple way to calculate the rock stress surrounding the workplace/roadway, but it needs accurate rock properties and in situ stress conditions (Xie et al. 2005). To simulate this big size model of ascending mining with complex geological conditions, numerical simulation is not the first choice. Mining physical simulation based on similarity theory and dimensional analysis is practiced easily and has a short model-making cycle, which has been widely used in the mining research in America, Australia, China, Poland, etc. (Gu 1995). Moreover, the physical model can almost simulate all kinds of geological conditions. Different ratios of similitude decide different engineering sizes. The key strata theory, a famous Chinese mining theory, has been tested and proved by this simulate method (Qian and Shi 2003; Chen and Qing 1994).

Therefore, this paper using physical simulation experiments, based on fractal geometry theory, in combination with the MATLAB software, studies the overburden rock crack distribution and evolution and fractal characteristics after mining-induced stress balance in order to control roadway surrounding rock as well as coal and gas simultaneous extraction safety and efficiency in ascending longwall mining.

## Physical model

The physical simulation experiment used the plane stress model frame (Fig. 1), whose geometric dimension (length  $\times$  width  $\times$  height) is 2,500 mm  $\times$  200 mm  $\times$  1,000 mm. The whole experimental system mainly includes three parts: framework system, loading system, and test systems.

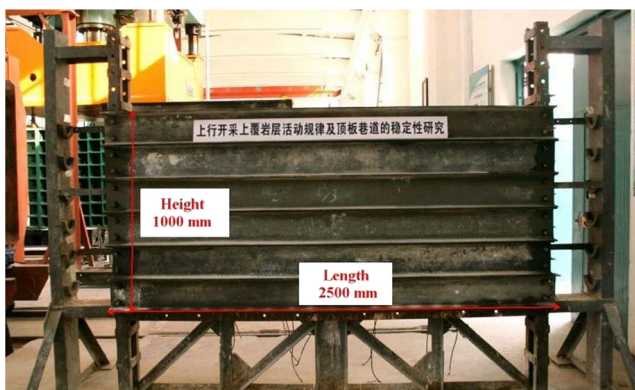


Fig. 1 The plane stress physical model frame

This model is a simulation of 1001 Workface at Taoyuan Coalmine in Huaibei Coal Mining Group of Anhui Province, China. The workface depth is 500 m underground. In accordance with the general physical phenomena requests, the physical simulation experiment should meet similar conditions: geometric similarity, movement similarity, stress similarity, dynamic similarity, and external condition similarity (Li 1988). According to model size and purpose of this study, the geometric similarity ratio of the model is determined to be  $C_l=100$  which could simulate actual size (length  $\times$  height, 250 m  $\times$  100 m). As the rock density is 2.5 g/cm<sup>3</sup> and the material density is 1.5 g/cm<sup>3</sup>, the density similarity constant is  $C_\rho=25/15$ , and the stress similarity constant is  $C_\sigma=100 \times 25/15=166.7$ . Since this model could only simulate the deepest depth of 100 m, the other 400-m overburden stress was loaded by a lever loading system, which could be calculated as follows:

$$\sigma_{el} = \frac{\rho g H}{C_\sigma} \quad (1)$$

where  $\sigma_{el}$  is the extra stress loaded by the loading system,  $\rho$  is the rock density (2.5 g/cm<sup>3</sup>),  $g$  is the acceleration due to gravity (9.8 N/kg),  $H$  is the extra actual depth which the model cannot simulate (400 m), and  $C_\sigma$  is the similar stress constant (166.7). According to Eq. (1), the extra load value is  $\sigma_{el}=60$  kPa.

When selecting various rock parameters of the model, the rock uniaxial compressive strength is the main similarity physical quantity which should be very close to real, and it is required that all other physical parameters should be approximately similar. The similar materials are made from sand, calcium carbonate, and gypsum in accordance with the ratio of the actual situation (Li 1988). The rock layers' material ratios are shown in Table 1.

The model-making process is shown in Fig. 2. First, measure all the materials with electronic scales accurately (Fig. 2a); then, mix them uniformly on a clean floor (Fig. 2b). After that, add the accurate value of water and mix them uniformly again (Fig. 2c). Finally, put the materials into the model frame according to the rock bed order in Table 1 from the bottom to the top and compact them with a hammer (Fig. 2d).

Remove the warp template a week after finishing the model; whitewash the model surface and draw grid lines airing it to dry. The grid size is 50 mm  $\times$  50 mm. Excavate 16 roadways with a cross-sectional size (width  $\times$  height) of 50 mm  $\times$  30 mm corresponding to the actual roadway size of 5,000 mm  $\times$  3,500 mm. The roadways of the model on the left labeled by nos. 1, 2, 5, 6, 7, 11, 12, and 13 used 30-mm-long bolts; the interrow spacing is 20 mm  $\times$  30 mm; and the remaining eight roadways are without support.

**Table 1** The mixture ratio of the similar materials and the dosage of each layer

Lithology	Ratio	Thickness/mm	Density/(g cm <sup>-3</sup> )	Compressive strength		Weight/kg			
				$\sigma_{cp}$ /MPa	$\sigma_{cm}$ /kPa	Sand	Calcium carbonate	Gypsum	Water
Siltstone	537	75	1.5	35	210	46.88	2.81	6.56	8.04
Mudstone	755	40	1.5	20	120	26.25	1.88	1.88	3.33
Seam 8 <sup>#</sup>	773	30	1.5	10	60	19.69	1.97	0.84	2.50
Sandy mudstone	555	100	1.5	25	1,150	62.50	6.25	6.25	8.33
Siltstone	537	40	1.5	35	210	25.00	1.50	3.50	3.33
Mudstone	755	60	1.5	18	108	39.38	2.81	2.81	5.00
Siltstone	537	60	1.5	35	210	37.50	2.25	5.25	5.00
Fine-grained sandstone	437	40	1.5	45	270	24.00	1.80	4.20	3.33
Sandy mudstone	555	150	1.5	25	150	93.75	9.38	9.38	12.50
Fine-grained Sandstone	437	80	1.5	45	270	48.00	3.60	8.40	6.67
Mudstone	755	80	1.5	18	108	52.50	3.75	3.75	6.67
Siltstone	537	100	1.5	35	210	62.50	3.75	8.75	8.33
Mudstone	755	50	1.5	18	108	32.81	2.34	2.34	4.17
Seam 10 <sup>#</sup>	773	35	1.5	10	60	22.97	2.30	0.98	2.92
Fine-grained Sandstone	437	60	1.5	45	270	36.00	2.70	6.30	5.00

Field observation shows that the horizontal distance of mining-induced stress influence area is around 60 m in 1001 Workface of Taoyuan Coalmine. Since the geometric similarity ratio of the model is  $C_l=100$ , considering the edge effect of the model, the cutoff site was chosen to be 650 mm from the left model edge and the same distance was chosen to the takeoff site from the right edge. The whole model length is

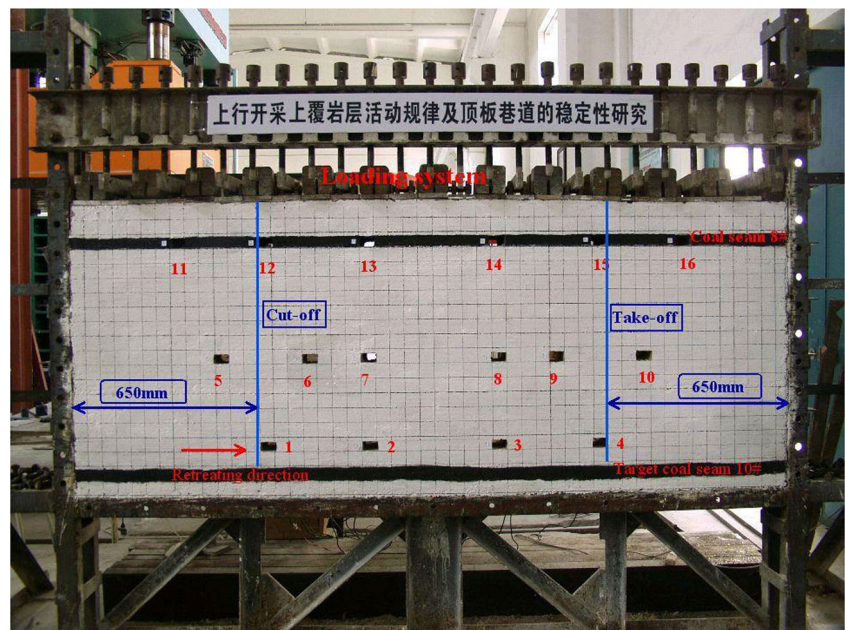
2,500 mm; therefore, the mining length is 1,200 mm, corresponding to the actual size of 120 m (Fig. 3).

Each excavation advances to 50 mm, a grid side length, which is 5 m in actual size corresponding to the mining speed of 5 m per day. The extraction time interval is 60 min. Usually, the physical simulation model would balance for 15~30 min after mining each interval (Tu et al. 2010).

**Fig. 2** The physical mode making process. **a** Measure the physical model materials, **b** mix the materials on a clean floor, **c** add weighed water in the materials and keep mixing uniformly, and **d** put the materials in the model frame and compact them with a hammer



**Fig. 3** The plane stress model frame and physical simulation model



### Analyses of overburden fracture evolution and roof destruction

#### Process of overburden breaking and collapse

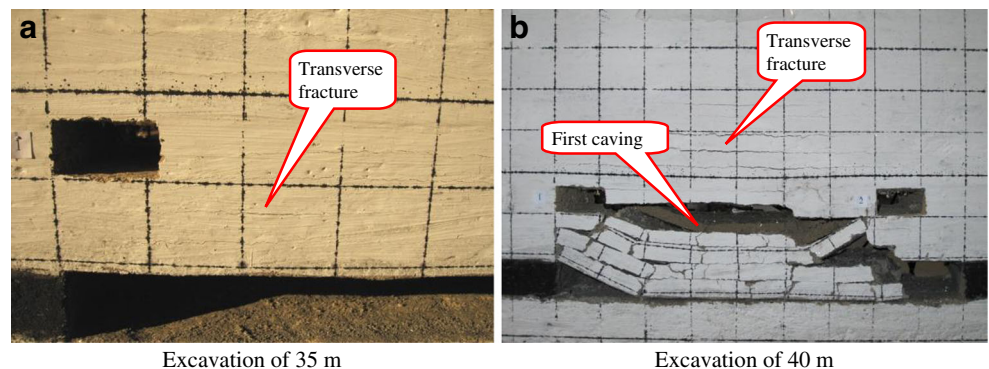
Face began to mine forward from the open-off cut. Rock stress gradually shifted to both sides of the coal wall near the working face. The hanging arch span of the immediate roof increased. After excavation of 35 m (Fig. 4a), the roof lateral fissure starts to develop fast, in which the number of cracks and the opening width increased significantly. With the development of lateral fissure, the immediate roof started to abscise from the roof, showing a weak bending, accompanied by micro-vertical cracks. When a 37.5-m depth was excavated, the immediate roof was partly caving, resulting in a large-scale breaking down of the first layer of immediate roof (fine-grained sandstone in Table 1) which is known as initial collapse when a 40-m depth was excavated (Fig. 4b). The caving

height is 6 m, in small blocks, and loosely shaped. The longitudinal crack and horizontal crack were present throughout the whole rock bed.

As the main roof strength is high, the roof arch is still hanging after the initial caving of immediate roof. Comparing with its overburden, the main roof deformation is large enough to separate from the overlying rock, forming a large suspended space supporting the overburden like plate (Zhang et al. 2013). Advancing to 55 m, the roof overhang reached its critical span and firstly broke and caved. Advancing to 75 m, the first periodic pressure happened. And since then, with each 20-m advancement, periodic weighting happened at a time, which caused a large scale of deformation and damage, as shown in Fig. 5.

As the roof rotates and sinks, the better lithology of the rock is the one with a lower degree of fragmentation after fracture, with integrity somehow. Roadways in better lithology rock

**Fig. 4** The initial collapse schematic of the immediate roof: **a** excavation of 35 m and **b** excavation of 40 m



Excavation of 35 m

Excavation of 40 m

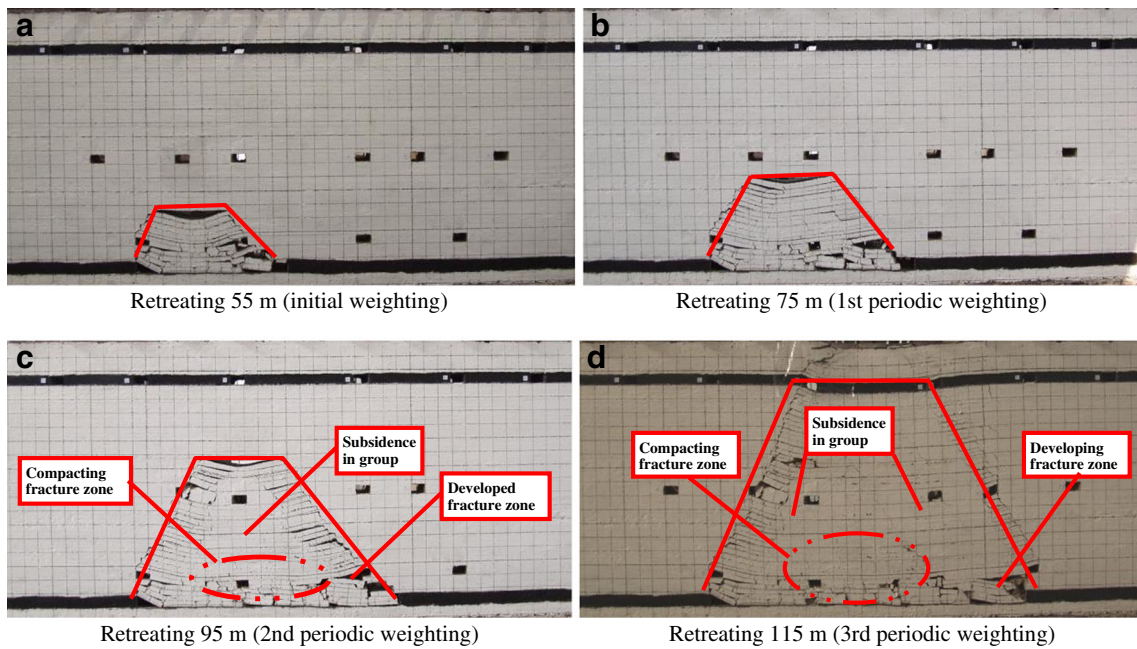


**Fig. 5** Overburden separation evolution: **a** retreating 55 m (initial weighting), **b** retreating 75 m (first periodic weighting), **c** retreating 95 m (second periodic weighting), and **d** retreating 115 m (third periodic weighting)

would have less deformation and failure, thus contributing to the maintenance of the roadway.

1. When the workface retreated to 38.8 m, there is an obvious pressure drop which indicated that the immediate roof began to cave (Fig. 6). The first stress peak appeared at 54.2 m, and this was the main roof caving and the first roof weighting. At the workface, you can hear rumbling noise in the upper roof.
2. The second peak came at 74 m from the cutoff site. This is the first periodic weighting of the roof; the second and the third periodic weightings were at 93.2 and 113.2 m from the open-off cut, respectively. Therefore, the periodic weighting pace is around 20 m which fits the physical experiment results very well.

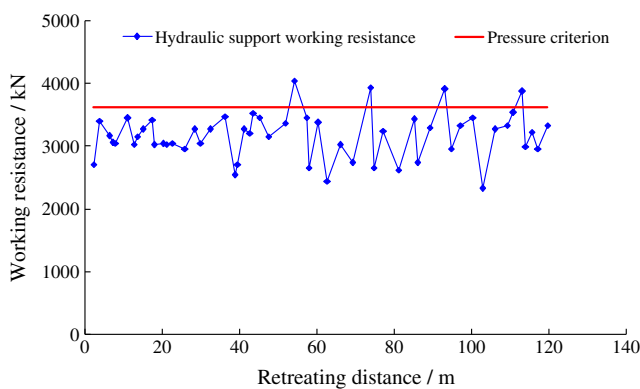


**Fig. 6** Hydraulic support working resistance versus retreating distance

### Separated strata rupture evolution

Figure 7 shows the overburden crack height while the workface advanced according to the records in Table 2.

Based on Figs. 5 and 7 and Table 2, the crack evolution of separated strata caving process is summarized as follows:

1. As the working face advanced, the overburden was trapezoidal damaged (Fig. 5) and forward and upward gradual evolution occurred. Cracks at the rear of working face experienced undeveloped, developing, full-compaction three phases. The cracks at 60 m behind the face were compressed, and the fissure-rich region was 30–50 m in the rear of the workface. The rock in the upper goaf was

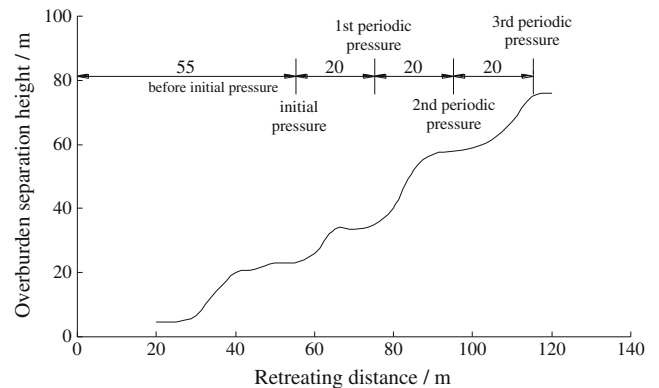


**Fig. 7** Relationship between overburden separation height and retreating distance

**Table 2** Relationship between overburden separation height and retreating distance

Advance distance/m	Separation height/m	Advance distance/m	Separation height/m	Advance distance/m	Separation height/m	Advance distance/m	Separation height/m
20	4.5	50	21	75	35	100	59
30	6.5	55	23	80	49	105	61.5
35	14	60	23	85	45	110	67
40	20	65	33.5	90	52	115	75
45	20	70	33.5	95	57	120	76

under shear stress, rotating and sinking to the goaf side. And roof fracture was constantly developing to the top rear  $45^\circ$  to  $50^\circ$  of the goaf. The abscission layer cracks and bias fissures closed at 50 m in the goaf to the workface. The tension cracks experience a dynamic process from open to close.

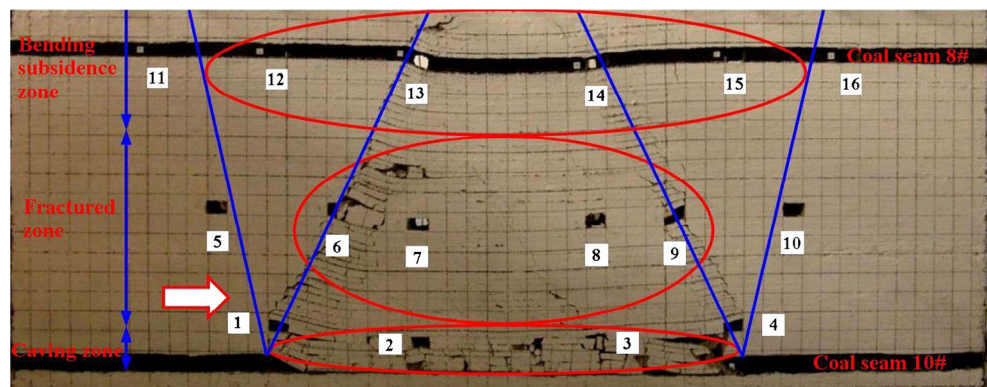
- The separated strata rupture is dynamic. With the face advancing, the separated layers developed upwards, the crack range was widened, and the rock rupture range expanded out following the same waveform line (Fig. 5).
- Within the overlying strata, multiple layers start to separate in group at the same time, so the rock moved and sunk with a sudden. The destruction of the lower parts of the rock makes the upper rocks fall apart.
- The crack height increased leapingly as the working face advanced, which is shown in Fig. 7. And the process is characterized by four stages: the stage before initial pressure, the stage affected by the initial pressure, the stage affected by the first periodic pressure, and the stage affected by the second periodic pressure. The abscission layer development height in each stage showed S-shaped growth trends (first was fast growth and then slow growth), and this growth trend was synchronized with the face weighting, but the increase speed of crack height was firstly increased and then decreased.
- The crack development increased intermittently with the face weighting, which intensified roadway damage, thus enabling the roadway to be destructive of a sudden. The

maintenance of the roadway is extremely difficult because of the poor safety situation.

#### The status of roadway roof destruction

With the advance of the workface, the overburden rock beds deform and destroy above the goaf. According to the damage degree of the roof rock, three zones could be divided, which are caving zone, fracture zone, and bending subsidence zone from the bottom to the top (Liu 1995; Qian and Shi 2003) (Fig. 8). The roof damage in different zones showed significant differences. From the analysis of simulation results, the following conclusions could be indicated:

- Caving zone. Bolting cannot maintain the roadway in the caving zone which behaves as a fallen strong roof and ground heave, due to serious damage of the roadway surrounding rock (Fig. 9a); the roof and floor of the roadway near the starting point of caving zone were overall shearing-dislocated and tilted to the goaf side; the roadway both with and without bolt support showed serious damage with small residual space and poor stability (Fig. 9b). The 50-mm $\times$ 35-mm roadway has been totally destroyed in the physical model which means that the 5,000-mm $\times$ 3,500-mm actual roadway would collapse completely.
- Fracture zone. The rock within the fracture zone sunk in group of multilayers with uneven subsidence; the lower

**Fig. 8** Overlying strata destruction and different roof failure zones

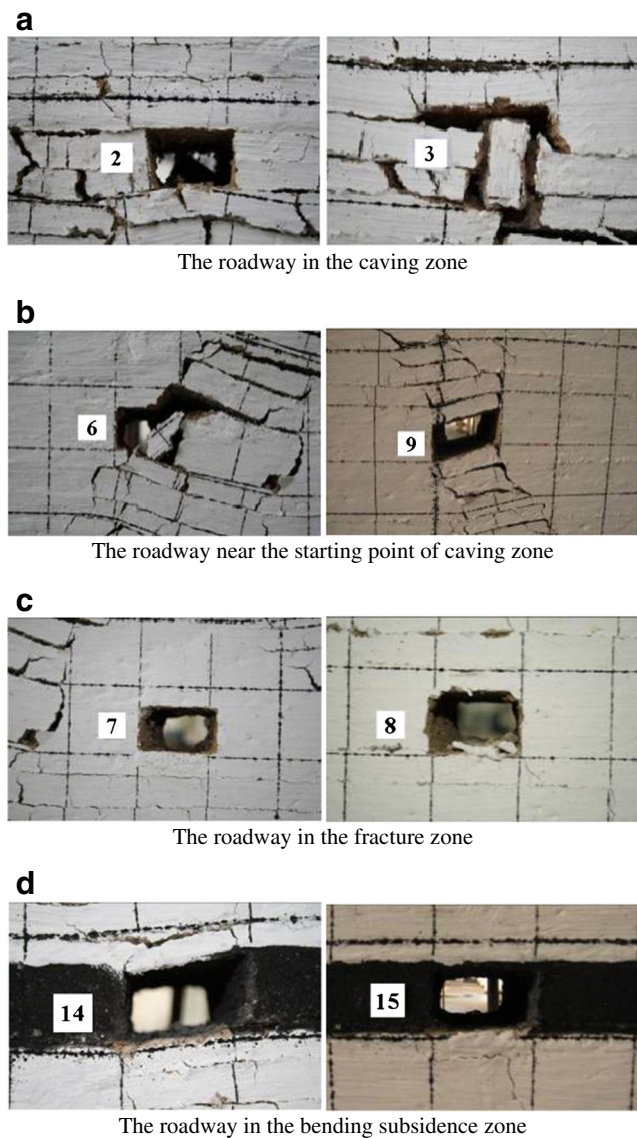


**Fig. 9** Failure and characteristics of roof roadway after mining: **a** the roadway in the caving zone, **b** the roadway near the starting point of caving zone, **c** the roadway in the fracture zone, and **d** the roadway in the bending subsidence zone

layers entirely sunk which allowed displacement of the upper rock. If the roadway allocated in sink area, the joints of the surrounding rock were significantly reduced. However, the damage of the surrounding rock in this region due to mining is still serious. The roadway is maintainable, but the overall stability is still poor and roof collapse is easy to take (Fig. 9c). This group failure sunk the whole roadway if it was contained in these sinking rock beds and the cracks are small; the roadway can be maintained through a variety of combinations of techniques.

3. Bending subsidence zone. This zone performed with rock sink as a whole, with less stratified shear dislocation. The roadway in this zone was less affected by mining-induced

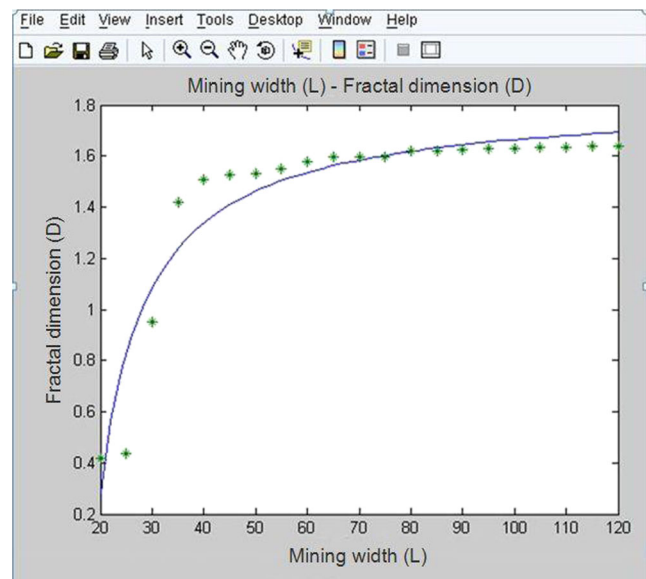


**Fig. 10** The relationship between fractal dimension and mining width

stress, as surrounding rock deformation and failure was not obvious. The bolt support showed a satisfied result, as shown in Fig. 9d.

**Fractal characteristics of overburden rock fractures**

The fractal dimension can reflect the placeholder of the cracks in the two-dimensional space, which characterizes the development degree of overburden rock fracture network by mining (Xie 1996; Sarkheil et al. 2011) In this paper, we used the overcast method, namely, the fractal theory, to study the rock fracture distribution map using a square mesh of  $R$  scale to cover the target area. The number of grids under which fracture length is equal and greater than the corresponding grid is counted and denoted by  $N(R)$ . An array of corresponding  $N(R)$  values can be obtained with a series of  $R$  values, to

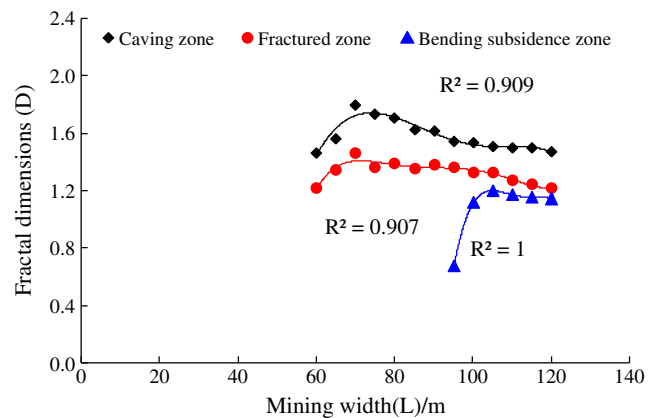


**Fig. 11** The relation between fractal dimensions and the three zones with different mining widths

study the relationship of the  $\log(R)$  and  $\log(1/R)$  (Yu et al. 1998) The fractal dimension  $D$  is defined as follows:

$$D = -\lim_{R \rightarrow 0} \frac{\log N(R)}{\log R} = \lim_{R \rightarrow 0} \frac{\log N(R)}{\log(1/R)} \quad (2)$$

A double-logarithmic plot, the best fit, can be plotted using the least square method; their relationship in the double logarithmic coordinates is basically linear and the negative value of the slope is the fractal dimension  $D$ . To get an accurate  $D$  value, the  $R$  values 2, 2.5, 5, 7.5, 10, 12.5, 15, and 20 (units are in centimeters) (Mandelbrot 1982; Wang et al. 2009) were chosen to study the relationship between the fractal dimension mining of rock mass fractures and the width of the mining face as well as the mentioned “three zones” (bending subsidence zone, fracture zone, and caving zone).

The relationship between fractal dimension and mining width

As the working face advanced, the rock mass of the roof and floor sequentially caved, displaced, and fractures and cracks emerged and closed. The upper roof rock also developed horizontal cracks and vertical cracks, so as to continuously produce new rock structures. The face advanced by 120 m at a rate of 5 m each time, which required 24 times of excavation. This gave a total of 24 different diagrams of cracks with mining widths, and the fractal dimensions were respectively calculated using the method mentioned above by MATLAB 7.0 software. Figure 10 was obtained, and the regression formula is as follows:

$$D = 1.8211 - \frac{4.2685}{(-3.201 + L/3.3220)^{1.0039}} \quad (3)$$

Figure 10 shows that the fractal dimension changes with the face retreating. It can be categorized into three stages:

1. In the first stage, when the mining width is less than 40 m, the fractal dimension  $D$  increases rapidly with the face advancement, reflecting the rapid development of the horizontal and vertical fracture network. This stage is called the fast dimension increase stage.
2. In the second stage, with 40–80-m range mining width, the fractal dimension  $D$  slowly increases with the face advancement, reflecting the rock mass fracture developing quickly at the front and the top of the working face and the top of the goaf. While at the same time, the fracture under the goaf roof closes, therefore the growth rate of the fractal dimension is smaller than the first stage. This stage is called the slow dimension increase stage, in which the crack development speed is slightly faster than the fracture closure speed.

3. In the third stage, when the mining width is more than 80 m, the changing rate of fractal dimension  $D$  is not noticeable; the value of  $D$  is basically stabilized, reflecting the developing speed of rock mass fracture at the front and the top of the working face and the top of the goaf is the same with the closure speed of the rock crack under the goaf roof. This stage is named the fractal dimension stable stage in which the fracture developing speed is about the same to closure speed.

The relationship between fractal dimension and the three zones

To push forward the distribution law of the fracture network in the three zones, the section that is 25–45 m away from the open cut was researched. The relationship variation between fractal dimension and the three zones with the face advancement (mining width) was calculated, as shown in Fig. 11.

The following conclusions can be concluded from Fig. 7:

1. With the face advancement, the fractal dimension  $D$  of the caving zone, the fracture zone, and the bending subsidence zone first increases rapidly; then, the increasing rate slows down, eventually stabilized. However, the three zones are not synchronous; bending subsidence zone lagged behind the fracture zone, while the fracture zone lagged behind the caving zone.
2. The fracture distribution and space occupying are different in the three zones. When mining width is the same, fractal dimension of the caving zone is greater than that of the fracture zone, while the fractal dimension of the fracture zone is greater than that of the bending-sinking zone, which indicates that the degree of space occupying increases in the order of the bending subsidence zone, the fracture zone, and the caving zone.

## Conclusions

Based on the physical simulation experiments, the fracture distribution and evolution of overburden rock beds in ascending mining were studied. The field observation results demonstrated that the physical models can simulate the actual engineering practice very well. Also, the fractal dimension was used to analyze the fracture distribution and evolution and the following conclusions were indicated:

1. The overburden rock was trapezoidal damaged, gradually breaking forward and upward, along with the rock deformation and caving in layer group. The fracture height developed by leaps and bounds discontinuously, making



roadway maintenance extremely difficult as there may be a sudden destruction.

2. The roadway roof is damaged by the dynamic effect of ascending mining, but the effect varies significantly with positions. The roadways near the starting point of the caving zone and those in the caving zone are not maintainable, those in the fracture zone can be maintained by a combination of technical means, while roadways in the curved sinking zone can be ideally supported with bolt support.
3. As the mining width increases, the fractal dimension of the crack network shows an overall staggered increasing trend, which is divided into rapid fracture dimension rising stage, slow fracture dimension rising stage, and fracture dimension stable stage.
4. The development, expansion, and closure of the fracture network in the caving zone, the fracture zone, and the bending subsidence zone are not synchronous; the bending zone lags behind the fracturing zone, while the fracture zone lags behind the caving zone, but there is a good inner similarity of the same trend in these three zones.

**Acknowledgments** We express our appreciation to the National Key Basic Research Development Program of China (2011CB201200), the National Natural Science Foundation of China (51304065), and the Doctor Foundation of Henan Polytechnic University (B2012-064) for their financial support.

## References

- Chen YG, Qing MG (1994) Strata control around coal face in China. China University of Mining and Technology Press, Xuzhou
- Cheng YP, Yu QX (2007) Development of regional gas control technology for Chinese coalmines. *J Min Saf Eng* 3:253–257
- Gu DZ (1995) Similar material and similar model. China University of Mining and Technology Press, Xuzhou
- Hu GZ, Wang HT, Li XH, Fan XG, Yuan ZG (2009) Numerical simulation of protection range in exploiting the upper protective layer with a bow pseudo-incline technique. *Min Sci Technol* 1:58–64
- Li HC (1988) Similar simulation test for ground pressure. China University of Mining and Technology Press, Xuzhou
- Li DZ, Xia XC, Han JG (2005) Deep mine mining technology. China University of Mining and Technology Press, Xuzhou
- Liu TQ (1995) Influence of mining activities on mine rock mass and control engineering. *J China Coal Soc* 1:1–5
- Liu CW, Guo YF, Yao JM (2003) The development and problems of mining similar—meaning of developing three dimensional mining physical simulation experiment. *China Min Mag* 8:6–8
- Liu QS, Zhang H, Lin T (2004) Study on stability of deep rock roadway in coal mines. *J Rock Mech Eng* 21:3732–3737
- Liu HB, Cheng YP, Song JC et al (2009) Pressure relief, gas drainage and deformation effects on an overlying coal seam induced by drilling an extra-thin protective coal seam. *Min Sci Technol* 6:724–729
- Ma ZG, Tu M, Ma JG et al (2008) Rock mass deformation characteristics for coal mining at remote lower protective. *J Min Saf Eng* 3:253–257
- Mandelbrot BB (1982) The fractal geometry of nature. Freeman, San Francisco
- Qian MG, Shi PW (2003) Ground pressure and strata control. China University of Mining and Technology Press, Xuzhou
- Sarkheil H, Hassani H, Alinia F (2011) Fractures distribution modeling using fractal and multi-fractal–neural network analysis in Tabnak hydrocarbon field, Fars, Iran. *Arab J Geosci* 6:945–956
- Tu SH, Ma WD, Wan ZJ et al (2010) Experimental method and measurement technique for ground control. China University of Mining and Technology Press, Xuzhou
- Wang C (2011) Study on control principle and key technologies for roof roadway stability of different zones in ascending mining condition. Doctoral Dissertation, China University of Mining and Technology
- Wang ZG, Zhou H-W, Xie HP (2009) Research on fractal characterization of mined crack network evolution in overburden rock stratum under deep mining. *Rock Soil Mech* 8:2403–2407
- Wang C, Zhang N, Li GC, Zhang NC (2011) De-stressed mining of multi-seams: surrounding rock control for mining influenced roadway in the overlying protected seam. *Int J Min Sci Technol* 2:159–164
- Xie HP (1996) Fractal rock mechanics introduction. Science, Beijing
- Xie WB, Chen XX, Zheng BS (2005) Numerical simulation research and analysis of mining engineering problem. China University of Mining and Technology Press, Xuzhou
- Ye JP, Shi BVS, Zhang CC (1999) Coal reservoir permeability and its controlled factors in China. *J China Coal Soc* 2:118–122
- Yu GM, Xie HP, Zhou HW et al (1998) Distribution law of cracks in structured rock mass and its experimental investigation. *J Exp Mech* 2:145–154
- Yuan L (2009) Technique of coal mining and gas extraction without coal pillar in multi-seam with low permeability. *J Coal Sci Eng* 2:120–128
- Zhang N, Zhang NC, Han CL et al (2013) Borehole stress monitoring analysis on advanced abutment pressure induced by Longwall Mining. *Arab J Geosci*. doi:10.1007/s12517-013-0831-7